materials

MDPI

Article

Copper-Zinc-Tin-Sulfur Thin Film Using Spin-Coating Technology

Min-Yen Yeh [1], Po-Hsun Lei [2,*], Shao-Hsein Lin [2] and Chyi-Da Yang [1]

[1] Department of Microelectronic Engineering, National Kaohsiung Marine University, Kaohsiung 811, Taiwan; minyen@mail.nkmu.edu.tw (M.-Y.Y.); cdyang@webmail.nkmu.edu.tw (C.-D.Y.)

[2] Institute of Electro-Optical and Materials Science, National Formosa University, 64 Wen-Hwa Rd, Hu-Wei, Yun-Lin 632, Taiwan; id7870.sl@gmail.com

* Correspondence: pohsunlei@gmail.com; Tel.:+886-5-6315668; Fax: +886-5-6329257

Academic Editor: Dirk Poelman

Received: 22 May 2016; Accepted: 27 June 2016; Published: 29 June 2016

Abstract: Cu_2ZnSnS_4 (CZTS) thin films were deposited on glass substrates by using spin-coating and an annealing process, which can improve the crystallinity and morphology of the thin films. The grain size, optical gap, and atomic contents of copper (Cu), zinc (Zn), tin (Sn), and sulfur (S) in a CZTS thin film absorber relate to the concentrations of aqueous precursor solutions containing copper chloride ($CuCl_2$), zinc chloride ($ZnCl_2$), tin chloride ($SnCl_2$), and thiourea ($SC(NH_2)_2$), whereas the electrical properties of CZTS thin films depend on the annealing temperature and the atomic content ratios of Cu/(Zn + Sn) and Zn/Sn. All of the CZTS films were characterized using X-ray diffraction (XRD), scanning electron microscopy (SEM), energy-dispersive X-ray spectroscopy (EDXS), Raman spectroscopy, and Hall measurements. Furthermore, CZTS thin film was deposited on an n-type silicon substrate by using spin-coating to form an Mo/p-CZTS/n-Si/Al heterostructured solar cell. The p-CZTS/n-Si heterostructured solar cell showed a conversion efficiency of 1.13% with V_{oc} = 520 mV, J_{sc} = 3.28 mA/cm^2, and fill-factor (FF) = 66%.

Keywords: CZTS thin film; solar cell; optical band gap; conversion efficiency

1. Introduction

Semiconductor solar cells incorporating thin-film absorbers are an attractive option for replacing classical silicon-based solar cells. In recent years, several thin-film absorbers such as III–V compound material (GaInP/GaAs) [1–3], I–III–VI compound material (Cu(In, Ga)Se_2, CIGS) [4–6], and I–II–VI compound material (Cu_2ZnSnS_4, CZTS) [7–9] have been investigated for semiconductor thin-film solar cells. Among these studied materials, direct band gap chalcopyrite-structured CIGS and kesterite-structured CZTS are potential absorber materials for the next generation of thin-film solar cells because of their large optical absorption coefficients over the visual light range. A record conversion efficiency of 20.3% was reported for a CIGS thin-film solar cell [4]. However, use of toxic Se and scarce or expensive elements, such as gallium (Ga) and indium (In), may limit the production development of CIGS thin-film solar cells. Researchers strongly desire to identify a nontoxic inexpensive thin-film absorber with high conversion efficiency to replace CIGS. CZTS has been considered as an alternative to CIGS because of its majority carrier type (p-type), direct band gap of 1.4–1.5 eV, and large optical absorption coefficient (>10^4 cm^{-1}) over the visible light range [10]. In addition, CZTS thin films are composed of elements that are nontoxic, abundant, and inexpensive, namely copper, zinc, tin, and sulfur.

CZTS thin films are generally fabricated using vacuum-based techniques such as thermal evaporation [11], sputtering [12], and pulsed laser deposition [13]. These methods can deposit high-quality CZTS thin films on molybdenum (Mo)-coated glass substrates. However, these techniques

require complicated equipment to maintain a vacuum and high process temperatures. In addition to high conversion efficiency, film content and composition as well as large-scale rather than small-area cell structural uniformity are challenges in developing CZTS thin-film solar cells for industrial use. Many nonvacuum methods of reducing production costs and satisfying the large-area requirements have been studied, including electrodeposition [14], spray pyrolysis techniques [15], sol-gel processing [16], spin-coating methods [17], and chemical bath methods [18]. Among these, the spin-coating method has the advantages of simple construction, low cost, ecological safety, and the large-scale deposition of different semiconductor thin films. However, few studies have reported the preparation of spin-coated CZTS thin films without toxic precursors such as hydrazine [19] or ethanolamine (MEA) [17]. Researchers do not completely and clearly understand the relationships of the deposition parameters to the atomic contents of Cu, Zn, Sn, and S, surface morphology, and electrical properties of spin-coated CZTS thin films.

In this study, we developed spin-coating Cu-poor and Zn-rich CZTS thin films with optimal atomic contents of Cu, Zn, Sn, and S onto glass and silicon (Si) substrates. The atomic contents of Cu, Zn, Sn, and S, crystalline morphology, and surface morphology of these CZTS thin films were characterized using energy-dispersive X-ray spectroscopy (EDX), X-ray diffraction (XRD) patterns, field-emission scanning electron microscopy (FE-SEM) images, and Raman measurements. The optical band gap and electrical properties were measured using absorption spectra and Hall measurements. Finally, an optimal CZTS thin was spun on an n-type Si substrate to form a Mo/p-CZTS/n-Si/Al solar cell.

2. Results and Discussion

The crystallinity, morphology, electrical properties, and band gap energy of CZTS thin films show a strong dependence on the stoichiometry of Cu, Zn, Sn, and S in those CZTS thin films [9,16,20–22]. Well-controlled atomic contents of Cu, Zn, Sn, and S in CZTS thin films has become a crucial issue for fabricating high-performance kesterite CZTS solar cells. To determine the optimal atomic contents of Cu, Zn, Sn, and S in CZTS thin films, the chemical concentrations of $CuCl_2$, $ZnCl_2$, $SnCl_2$, and thiourea aqueous precursor solution should be analyzed. Figure 1a–d show the atomic content ratios of Cu/(Zn + Sn), Cu/Zn, Zn/Sn, and S/(Cu + Zn + Sn) for CZTS thin films as functions of the concentrations of $CuCl_2$, $ZnCl_2$, $SnCl_2$, and thiourea aqueous precursor solution, respectively, for an annealing temperature of 350 °C. As shown in Figure 1a–c, the atomic contents of Cu, Zn, and Sn increase with raising the concentration of $CuCl_2$, $ZnCl_2$, and $SnCl_2$ aqueous precursor solution, respectively, implying that the atomic contents of Cu, Zn, Sn, and S in CZTS thin films can be modulated by changing the concentrations of aqueous precursor solution. Cu-rich CZTS thin films can facilitate the formation of passivated defect clusters such as Cu_{Zn} + Sn_{Zn} and $2Cu_{Zn}$ + Sn_{Zn}. The former produces a deep donor level in the band gap of CZTS, whereas the latter can significantly reduce the band gap of CZTS [20]. However, a high Zn/Sn ratio or high Zn atomic content is necessary to form the Zn_{Sn} acceptors and reduce the Sn_{Zn} donors to increase the conductivity of the CZTS thin film [23]. However, high Zn atomic content, which results in a low Cu/Zn ratio, can bring about a p/n conduction type [22]. To avoid defect clusters and increase the conductivity of p-type CZTS thin films, the Cu/(Zn + Sn) atomic content ratio should be less than 1, the Zn/Sn atomic content ratio should be more than 1, and the Cu/Zn atomic content ratio should not be too low. In Figure 1a, the atomic content ratio of Cu/(Zn + Sn) is lower than 1 for the $CuCl_2$ concentration below 0.14 M and approaches 1 at the $CuCl_2$ concentration of 0.16 M. When the $ZnCl_2$, $SnCl_2$, and thiourea concentrations increase with a $CuCl_2$ concentration of 0.14 M, the Cu/(Zn + Sn) atomic content ratio remains below 1, as seen in Figure 1b–d. These results indicate that Cu-poor and Zn-rich CZTS thin films can be produced from properly controlled concentrations of aqueous precursor solutions. The atomic content ratio of S/Cu + Zn + Sn in CZTS thin films can approach 1 for the concentrations of $CuCl_2$, $ZnCl_2$, and $SnCl_2$, as shown in Figure 1a–c, respectively. In addition, in Figure 1d, the atomic content of S increases

slightly as the thiourea concentration rises from 0.6 to 0.8 M, and saturates at a thiourea concentration above 0.8 M, possibly because of the solubility of S in the CZT thin film.

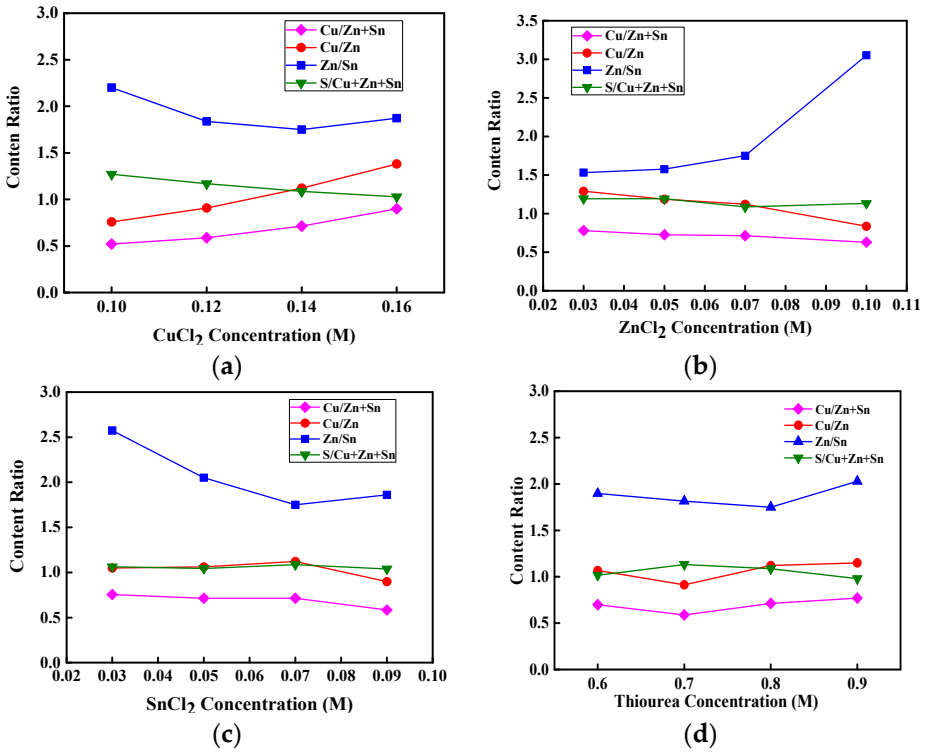

Figure 1. Atomic content ratios of Cu/(Zn + Sn), Cu/Zn, Zn/Sn, and S/(Cu + Zn + Sn) for copper-zinc-tin-sulfur (CZTS) thin films with (**a**) $CuCl_2$; (**b**) $ZnCl_2$; (**c**) $SnCl_2$; and (**d**) thiourea concentrations, respectively.

Figure 2a–c represent the XRD patterns for films with various concentrations of $CuCl_2$, $ZnCl_2$, and $SnCl_2$ aqueous precursor solutions that were annealed at a temperature of 350 °C. The XRD peaks were indexed using JADE software (Jade 5.0, Christchurch, New Zealand) as the CZTS kesterite structure; and they closely matched the standard data (PDF#26-5075). All of the spin-coated CZTS thin films exhibited a polycrystalline kesterite crystal structure with six broad peaks along the (101), (112), (200), (220), (312) and (224) planes as shown in Figure 2a–c. The secondary phases including Cu_2SnS_3, CuS, SnS and ZnS would form during growth of CZTS thin films. They will degrade the performance of CZTS solar cells. It is important to avoid the formation of secondary phases in CZTS thin films. Among these secondary phases, tetragonal-structured Cu_2SnS_3 (PDF#33-0501) and cubic-structured ZnS (PDF#05-0566) show the similar XRD patterns to kesterite-structured CZTS between diffraction angles of 20 and 80 degrees because of the same lattice constants [15]. As a result, the measured XRD patterns of CZTS thin film might be related to either CZTS or Cu_2SnS_3 or ZnS pahse. The weak peak at 18.2° attributed to (101) plane indicates a kesterite-structured CZTS thin film because it is not found in the XRD patterns of tetragonal-structured Cu_2SnS_3 and cubic-structured ZnS. Consequently, a CZTS thin film without secondary phase, which leads to a degraded performance of CZTS solar cells, can be obtained using properly controlled concentrations of aqueous precursor solutions and a proper annealing process. To further confirm the XRD characteristics of this spin-coated CZTS thin film, which differ from similar XRD patterns such as those of ZnS and Cu_2SnS_3, Raman spectroscopy was performed. Figure 2e shows the Raman spectrum for a spin-coated CZTS thin film prepared from 0.14 M $CuCl_2$, 0.07 M $ZnCl_2$, 0.07 M $SnCl_2$, and 0.8 M thiourea aqueous precursor solutions and annealed at 350 °C. The characteristic CZTS peak in Figure 2e is at 336.2 cm^{-1}, which is different from

the Raman peaks of $Cu_{2-x}S$ at 475 cm^{-1}, ZnS at 273 and 351 cm^{-1}, Cu_2SnS_3 at 290 and 352 cm^{-1}, and of Sn_2S_3 at 234 and 307 cm^{-1}, indicating a spin-coated CZTS thin film deposited on glass substrate [24,25].

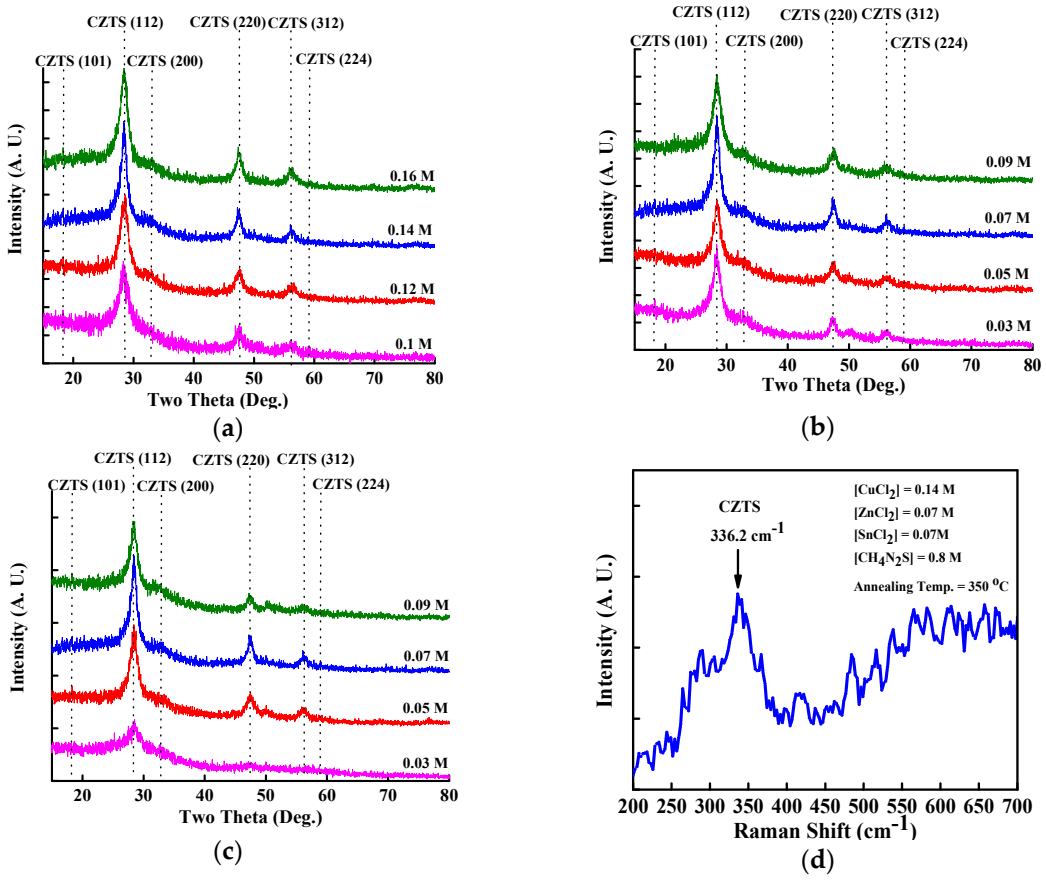

Figure 2. X-ray diffraction (XRD) patterns for CZTS thin film with varied concentration of (**a**) $CuCl_2$; (**b**) $ZnCl_2$; and (**c**) $SnCl_2$ aqueous precursor solution under an annealing temperature of 350 °C. The Raman spectrum for a CZTS thin film with $CuCl_2$, $ZnCl_2$, $SnCl_2$, and thiourea aqueous precursor solution concentration of 0.14, 0.07, 0.07, and 0.8 M, respectively, after annealing at 350 °C is shown in (**d**).

The mean crystallite grain size (D) of CZTS thin film can be estimated by the Scherrer formula [26]:

$$D = c\frac{0.9\lambda}{\beta\cos\theta} \quad (1)$$

where β, λ, and θ_B are the line width at full width at half the maximum of the film diffraction peak at 2θ, X-ray wavelength (0.15406 nm), and Bragg diffraction angle, respectively. Figure 3a–c show the full width at half maximum (FWHM) of (112) peak and calculated mean crystallite grain size of CZTS thin films as a function of the varied concentration of $CuCl_2$, $ZnCl_2$, and $SnCl_2$ aqueous precursor solutions that were annealed at a temperature of 350 °C. The grain size enlarges with increasing $CuCl_2$ concentration, as shown in Figure 3a because of the increase of Cu atomic content in the CZTS thin films [27,28]. This increase in the grain size might be due to agglomeration of grains. In addition, the grain size of CZTS thin films represents a slight change as $ZnCl_2$, and $SnCl_2$ concentrations increase or decrease while $CuCl_2$ concentration is maintained at 0.14 M, as shown in Figure 3b,c. This is attributed to the fairly constant Cu atomic content in these CZTS thin films. Consequently, the grain size of CZTS thin films with the same annealing temperature is determined by the Cu atomic content.

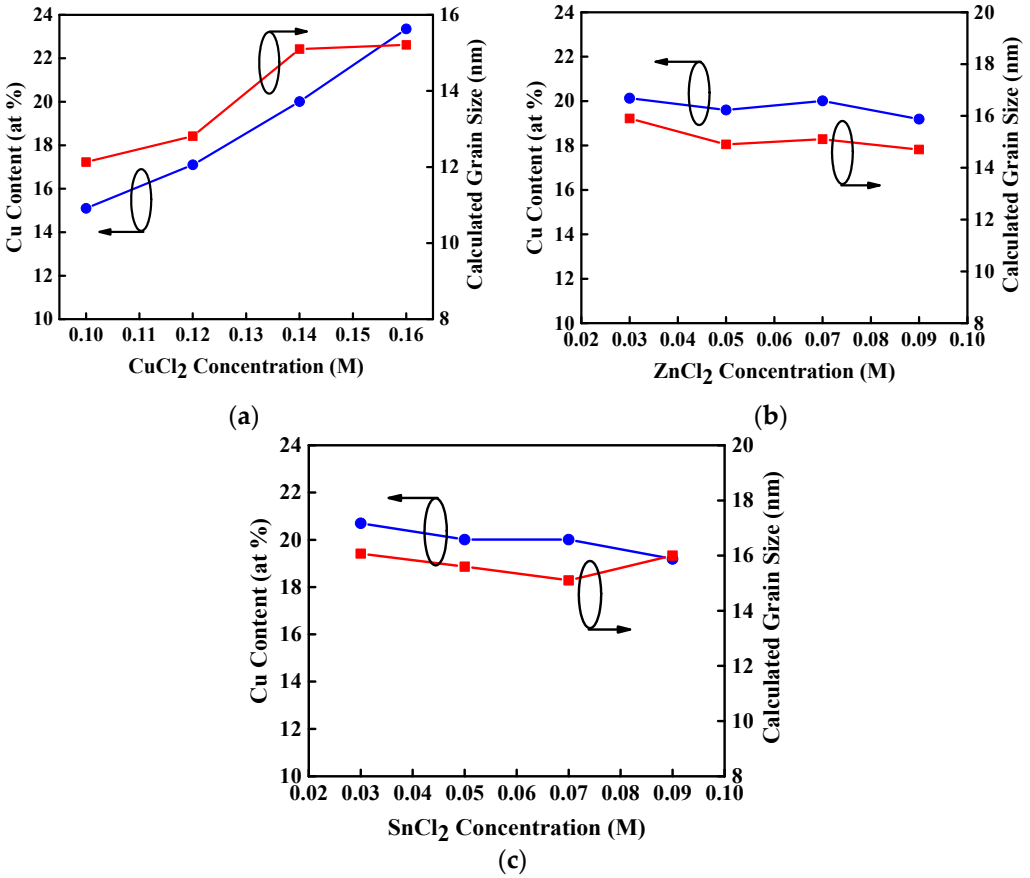

Figure 3. Full width at half maximum (FWHM) of (112) peak and calculated grain size for CZTS thin films with varied concentration of (**a**) $CuCl_2$; (**b**) $ZnCl_2$; and (**c**) $SnCl_2$ aqueous precursor solution under an annealing temperature of 350 °C.

The conversion efficiency of a CZTS thin-film solar cell is strongly associated with the grain size because an absorber layer with a large grain size maximizes the minority carrier diffusion length and the inherent potential of a polycrystalline solar cell [16,24]. Figure 4 shows the FE–SEM images of the CZTS thin film. Figure 4a–c show plane views of CZTS thin films with $CuCl_2$ concentrations of 0.1, 0.14, and 0.16 M with concentrations of $ZnCl_2$, $SnCl_2$, and thiourea at 0.07, 0.07, and 0.8 M, respectively. The thickness of all the CZTS thin films was approximately 2.4 µm, and Figure 4d represents the FE-SEM cross section image of CZTS thin film with concentrations of $CuCl_2$, $ZnCl_2$, $SnCl_2$, and thiourea at 0.14, 0.07, 0.07, and 0.8 M. As shown in Figure 4a–c, large numbers of voids were observed in the Cu-rich CZTS thin films. Voids of Cu-rich CZTS absorbers in thin-film solar cells cause low conversion efficiencies for photovoltaic applications [16,29]. Well-controlled Cu atomic content is important to obtain a large grain size and less number of voids in CZTS thin films. Figure 4e shows the plane view of a CZTS thin film with a high $ZnCl_2$ concentration of 0.1 M and $CuCl_2$, $SnCl_2$, and thiourea concentrations of 0.14, 0.07, and 0.8 M. The surface of Zn-rich CZTS thin film is smoother than that of Zn-poor CZTS thin films because of the large columnar grains at the bottom [30].

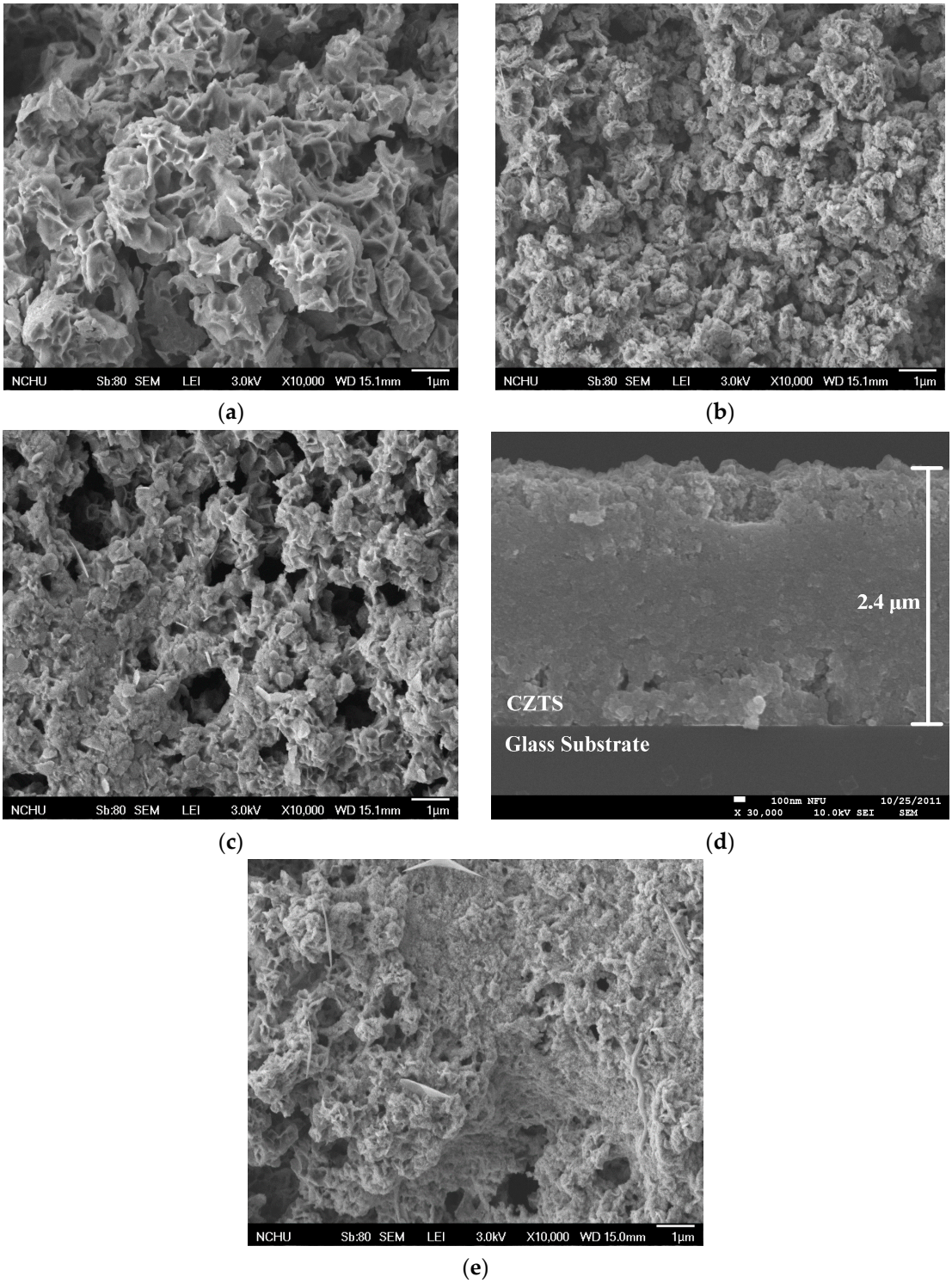

Figure 4. Plane-view field-emission scanning electron microscopy (FE–SEM) images of CZTS thin films deposited with $ZnCl_2$, $SnCl_2$, and thiourea concentrations of 0.07, 0.07, and 0.8 M, respectively, and $CuCl_2$ concentrations of (**a**) 0.1 M; (**b**) 0.14 M; and (**c**) 0.16 M, respectively. The cross section image of a CZTS thin film with $CuCl_2$, $ZnCl_2$, $SnCl_2$, and thiourea concentrations of 0.14, 0.07, 0.07, and 0.8 M is represented in (**d**). A CZTS thin film fabricated with $ZnCl_2$, $SnCl_2$, $CuCl_2$, and thiourea concentrations of 0.1, 0.07, 0.14, and 0.8 M, respectively, is shown in (**e**).

Figure 5 shows the graph of optical band gap energy as a function of the Cu/(Zn + Sn) atomic content ratio. The optical band gaps of these CZTS thin films range from 1.39 to 1.69, whereas the Cu/(Zn + Sn) atomic content ratios range from 0.58 to 0.76. This shift is attributed to the change in the p-d hybridization between Cu d-levels and S p-levels [16]. In addition, the relation of the extended optical band gap to the decrease in grain size is attributed to the fact that the band gap energy of a material is dependent on the particle size of that material according to the quantum size effect [15]. As shown in Figure 3a–c, the grain size of a Cu-poor CZTS thin film is smaller than that of a Cu-rich CZTS thin film, resulting in a wide optical band gap. The inset of Figure 5 shows a plot of $(\alpha h\nu)^2$ against the photon energy of a Cu-poor and Zn-rich (Cu/Zn = 1.12) CZTS thin film where α is the absorption coefficient and $h\nu$ is the photon energy. The optical band gap energy is estimated by extrapolating the linear region in the $(\alpha h\nu)^2$ plot and determining the intercept with the photon energy axis. The optical band gap for an optimal CZTS absorber is approximately 1.5 eV.

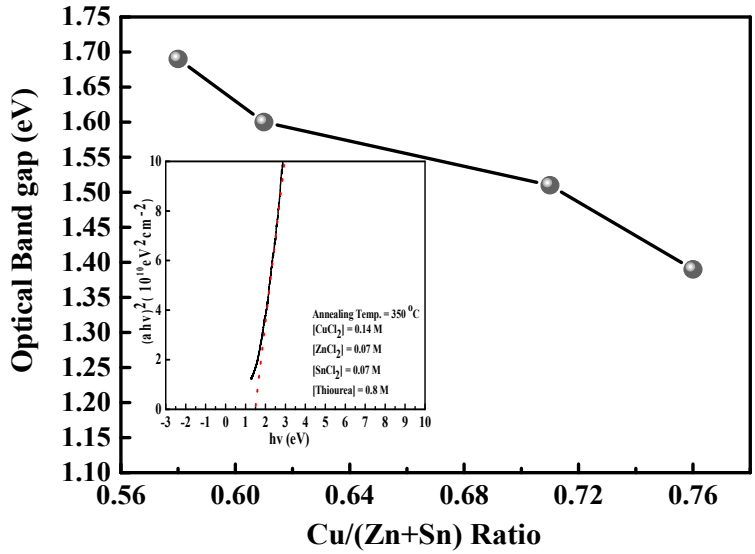

Figure 5. Optical band gap as a function of the Cu/(Zn + Sn) ratio, and the inset shows the plot of $(\alpha h\nu)^2$ against the photon energy of a Cu-poor and Zn-rich (Cu/Zn = 1.12) CZTS thin film.

Figure 6a,b show the carrier concentration and resistivity of CZTS thin films as a function of $CuCl_2$ and $ZnCl_2$ concentration, respectively. The carrier concentration shown in Figure 6a increases with $CuCl_2$ concentration. The formation of a Cu_{Zn} + Sn_{Zn} deep level depends on the Cu/(Zn + Sn) and Zn/Sn atomic content ratio, and an optimal condition occurs at Cu/(Zn + Sn) ≈ 0.8 and Zn/Sn ≈ 1.2 [20]. As the $CuCl_2$ concentration increases from 0.1 to 0.14 M, the Cu/(Zn + Sn) atomic content ratio approaches the optimal value because of the suppression of the formation of a Cu_{Zn} + Sn_{Zn} deep donor level in the CZTS band gap, leading to a significant increase in hole concentration. Nevertheless, the Cu/(Zn + Sn) atomic content ratio increases with $CuCl_2$ concentration to 1.6 M, causing the generation of a Cu_{Zn} + Sn_{Zn} deep donor defect and a reduction of the Cu_{Zn} antisite acceptor defects, resulting in a decrease of carrier concentration. Under the optimal Cu/(Zn + Sn) atomic content ratio of 0.714, the CZTS thin film has a high carrier concentration of 1.07×10^{19} cm^{-3} and a resistivity of 1.19 Ωcm. The atomic content ratio of Zn/Sn is also a crucial factor determining the electrical properties of a CZTS thin film. The Zn_{Sn} antisite defect with an inherent p-type conduction type in a CZTS thin film can easily form under a high Zn/Sn atomic content ratio. However, further increases in Zn/Sn atomic content ratio would generate a large population of intrinsic defects, causing a detrimental influence relative to a CZTS thin film with a atomic content ratio of Cu/(Zn + Sn) = 1 and Zn/Sn = 1. In Figure 6b, the hole concentration decreases as the $ZnCl_2$ concentration rises from 0.7 to 0.9 M because of the population of donor defect clusters [20]. Further increases in $ZnCl_2$ concentration

would move the Cu/(Zn + Sn) atomic content ratio away from 0.8 (see Figure 1b), leading to a translation of conduction types.

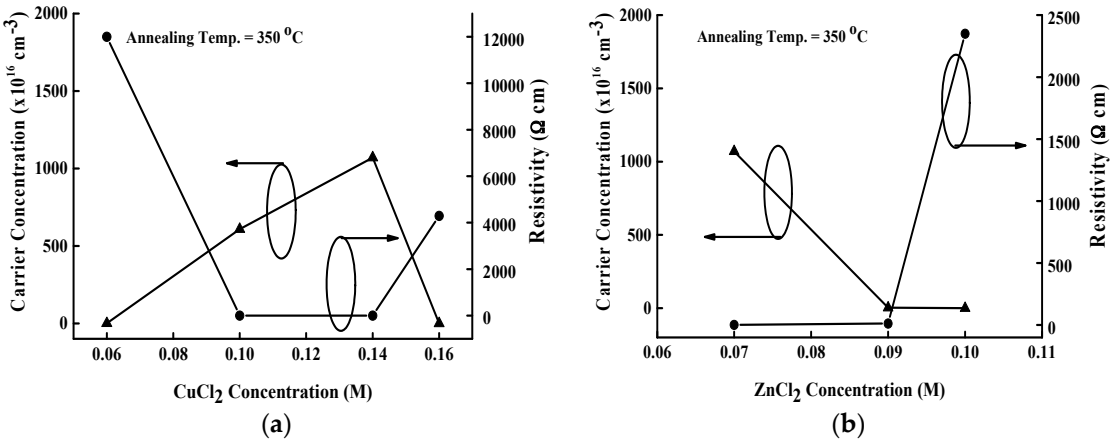

Figure 6. Carrier concentration and resistivity of the CZTS thin film as a function of the (**a**) $CuCl_2$; and (**b**) $ZnCl_2$ concentrations.

The sulfer vacancy (V_S) is also a dominant donor-like defect in a CZTS thin film because of its low formation energy. The conduction type would change from p-type to n-type and the hole concentration might decrease in an S-poor CZTS thin film due to a high concentration of V_S. High S content or S-rich in CZTS thin film is crucial to reduce the concentration of V_S. Kosyak et al. [31] have calculated the concentration of Zn_{Sn} antisite and V_S in CZTS thin films with different Cu, Zn, and Sn content, and represented that the concentration of acceptor-like Zn_{Sn} antisite is higher than that of donor-like V_S in a Zn-rich and Sn-poor CZTS thin film. Based on this result, we measure the electrical properties of CZTS thin films with various thiourea concentration under optimal Cu/(Zn + Sn) atomic content ratio of 0.714. Table 1 lists the measured results of S/(Cu + Zn + Sn) atomic content ratio and electrical characteristics of CZTS thin films depending on various thiourea concentration. The S/(Cu + Zn + Sn) atomic content ratio increases with rising thiourea concentration, implying that the a high S content or S-rich CZTS thin film can be obtained by changing the concentration thiourea aqueous solution. As thiourea concentration rises from 0.6 to 0.8 M, the hole concentration and conductivity of the p-type CZTS thin film increase because of reduction of V_S concentration. However, further increase in thiourea concentration would reduce the hole concentration and conductivity possible due to the formation of ZnS [32].

Table 1. The S/(Cu + Zn + Sn) atomic content ratio and electrical characteristics of copper-zinc-tin-sulfur (CZTS) thin films with different thiourea concentration.

Thiourea Concentration (M)	S/(Cu + Zn + Sn)	Conduction Type	Carrier Concentration (cm^{-3})	Mobility (cm^2/Vs)	Resistivity (Ùcm)
0.6	1.04	p/n	9.13×10^{17}	0.34	20.7
0.7	1.07	p/n	1.32×10^{18}	0.22	19.2
0.8	1.09	p	1.07×10^{19}	0.49	1.19
0.9	1.19	p	8.87×10^{18}	0.55	1.23

Table 2 shows the relation between annealing temperature and conduction type, carrier concentration, mobility, and resistivity of CZTS thin films with concentrations of $CuCl_2$, $ZnCl_2$, $SnCl_2$, and thiourea aqueous precursor solution at 0.14, 0.07, 0.07, and 0.8 M, respectively. The hole concentration for annealing temperatures of 300 °C, 350 °C, 400 °C, and 450 °C are 2.02×10^{14}, 1.07×10^{19}, 2.80×10^{15}, and 1.24×10^{16} cm^{-3}. The varied carrier concentrations of CZTS thin films

with increasing annealing temperatures is attributed to the changes of Cu/(Zn + Sn) and Zn/Sn content ratios, which cause the formation of Cu_{Zn} + Sn_{Zn} deep donor defects by reducing the Cu_{Zn} antisite acceptor defects [20,25]. The mobility of CZTS thin films shows a counterclockwise dependence on the carrier concentration because of the impurity scattering. In conclusion, with an annealing temperature of 350 °C, CZTS thin films have a stable p-type conduction type with a high hole concentration of 1.07 × 10^{19} cm^{-3} and a low resistivity of 1.19 Ωcm. To realize the optimal CZTS absorber for photovoltaic solar cell applications, a CZTS thin film was spin-coated onto an Si substrate to fabricate a Mo/p-CZTS/n-Si/Al heterostructured solar cell.

Table 2. Temperature dependence of conduction type, carrier concentration, mobility, and resistivity of the CZTS thin film measured using Hall measurements.

Annealing Temperature (°C)	Conduction Type	Carrier Concentration (cm^{-3})	Mobility (cm^2/Vs)	Resistivity (Ùcm)
300	p/n	2.02 × 10^{14}	126	245
350	p	1.07 × 10^{19}	0.49	1.19
400	p/n	2.80 × 10^{15}	7.95	280
450	p/n	1.24 × 10^{16}	0.094	5310

Figure 7 shows the (current-voltage) *I–V* characteristics of this Mo/CZTS/Si/Al solar cell under (air mass) AM 1.5 G. The open circuit voltage, short current density, fill factor, and efficiency were 520 mV, 3.28 mA/cm^2, 66%, and 1.13%, respectively. The Mo/CZTS/Si/Al heterostructured solar cell prepared in this work was simple and the characteristics of the CZTS thin film used as the absorber in this solar cell should be investigated as soon as possible. Compared with the techniques of preparing CZTS thin films reported by other authors, our CZTS thin film preparation method of using spin-coating exhibits superior performance for photovoltaic solar cell applications.

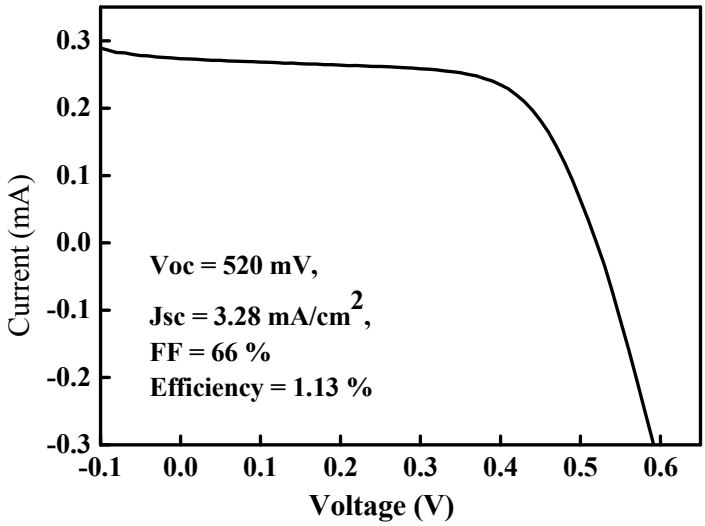

Figure 7. Current-voltage (*I–V*) characteristics of a Mo/CZTS/Si/Al heterostructured solar cell under (air mass) AM 1.5 G.

3. Experimental Details

3.1. Preparation of CZTS Thin Film

Because the solubility levels of $CuCl_2$, $ZnCl_2$, $SnCl_2$, and thiourea powder in deionized (DI) water differ, these powders were dissolved in DI water individually to form aqueous precursor solutions with varied molar concentrations. If the aqueous precursor solutions do not contain toxic organic

materials, such as MEA, spin-coating them uniformly onto glass substrates can be difficult. To spread precursor solutions uniformly without using toxic materials, the surfaces of the glass substrates were modified by using plasma cleaning to generate hydrophilic surfaces. To increase the S content of the CZTS thin film and prevent the mixed aqueous solution from becoming turbid, two separate spin-coating steps were applied to deposit CZTS thin films. For the first step, $CuCl_2$, $ZnCl_2$, and $SnCl_2$ aqueous precursor solutions were mixed and stirred uniformly to form a metallic aqueous solution that was spin-coated onto soda lime glass substrates. The glass substrates, coated with uniformly distributed metallic aqueous solution, were treated using thermal processes, namely baking on a hot plate at 100 °C for 3 min to dewater and annealing in a furnace at 350 °C for 5 min to tailor the crystallinity and morphology of the CZT layer. In the second step, aqueous thiourea solution was spun onto the CZT layers, and then the samples were treated by being baked on a hot plate for 3 min at 100 °C. Then, thermal annealed in a furnace for 180 min at 350 °C to form CZTS thin films. The surface morphologies of the CZTS thin films were characterized using FE-SEM and XRD patterns by using a Bruker D8 advanced diffractometer (XRD: Bruker AXS-DS Discov, Taichung Taiwan) equipped with a CuKá (λ = 0.154 nm). The atomic contents of Cu, Zn, Sn, and S in these CZTS thin films were measured using EDX with the same diffractometer. The absorption of CZTS thin films in the visual range was measured using a UV–Vis–NIR spectrophotometer (UVD-350, Yunlin Taiwan). The electrical properties of CZTS thin films, including carrier concentration, carrier mobility, and resistivity, were measured using Hall measurements (HMS-5000) at room temperature.

3.2. Fabrication of the Mo/CZTS/n-Si/Al Heterostructured Solar Cell

The preparation of the Mo/p-CZTS/n-Si/Al heterostructured solar cell can be described as follows. First, aluminum (Al) metal was deposited on the back of an n–Si substrate using a thermal evaporation process and then a thermal annealing treatment was applied to the sample to form an ohmic contact between Si and Al. Second, the optimal CZTS absorber layer was deposited on the surface of the n-Si substrate through spin-coating, followed by a thermal annealing procedure. Third, the Mo metal was sputtered onto the CZTS absorber contact region to serve as ohmic contact metal. The sample was then annealed in N_2 atmosphere for 5 min at 400 °C.

4. Conclusions

In this study, we spin-coated CZTS thin films onto glass substrates and annealed them to improve the crystallinity and morphology of the thin films. The amounts of Cu, Zn, Sn, and S in these CZTS thin films depend on the $CuCl_2$, $ZnCl_2$, $SnCl_2$, and $SC(NH_2)_2$ concentrations of the precursor solutions. The surface morphology and optical band gap properties of these CZTS thin films relate to the Cu content and the electrical properties of these CZTS thin films depend on the annealing temperature and the Cu/(Zn + Sn) and Zn/Sn ratios. All of the CZTS thin films exhibited a polycrystalline kesterite crystal structure with three major broad peaks along the (112), (220), and (312) planes in XRD patterns. The optimal CZTS thin film can be deposited on a glass and Si substrate with proportions of $[CuCl_2]$ = 0.14 M, $[ZnCl_2]$ = 0.07 M, $[SnCl_2]$ = 0.07 M, and $[SC(NH_2)_2]$ = 0.8 M and an annealing temperature of 350 °C. Finally, an optimal CZTS thin film was deposited on an n-type silicon substrate to produce a Mo/p-CZTS/n-Si/Al heterostructured solar cell with a conversion efficiency of 1.13% and with V_{oc} = 520 mV, J_{sc} = 3.28 mA/cm^2, and fill-factor (FF) = 66%.

Acknowledgments: The authors gratefully acknowledge the financial support of the Ministry of Science and Technology, R.O.C. (101-2622-E-150-013-CC3).

Author Contributions: Min-Yen Yeh and Po-Hsu Lei organized and designed the experiment procedure, and wrote the paper. Shao-Hsein Lin execute the deposition of CZTS thin films. Chyi-Da Yang performed the measurement of CZTS thin films. All of the authors read and approved the final version of the manuscript to be submitted.

Conflicts of Interest: The authors declare that there is no conflict of interests.

References

1. Nelson, J. *The Physics of Solar Cells*; Imperial College Press: London, UK, 2003; p. 211.
2. Shahrjerdi, D.; Bedell, S.W.; Ebert, C.; Bayram, C.; Hekmatshoar, B.; Fogel, K.; Lauro, P.; Gaynes, M.; Gokmen, T.; Ott, J.A.; et al. High-efficiency thin-film InGaP/InGaAs/Ge tandem solar cells enabled by controlled spalling technology. *Appl. Phys. Lett.* **2012**. [CrossRef]
3. Lei, P.H.; Lin, C.T.; Ye, S.J. Improved efficiency of GaInP/(In)GaAs/Ge solar cells using textured liquid-phase-deposited (LPD) ZnO. *J. Phys. D Appl. Phys.* **2012**. [CrossRef]
4. Jackson, P.; Hariskos, D.; Lotter, E.; Paetel, S.; Wuerz, R.; Menner, R.; Wischmann, W.; Powalla, M. New world record efficiency for Cu (InGa)Se_2. *Prog. Photovol. Res. Appl.* **2012**, *19*, 894–897. [CrossRef]
5. Wada, T.; Nakamura, S.; Maeda, T. Ternary and multinary Cu-chalcogenide photovoltaic materials from $CuInSe_2$ to Cu_2ZnSeS_4 and other compounds. *Prog. Photovol. Res. Appl.* **2012**, *20*, 520–525. [CrossRef]
6. Zhou, D.; Zhu, H.; Liang, X.; Zhang, C.; Li, Z.; Xu, Y.; Chen, J.; Zhang, L.; Mai, Y. Sputtered molybdenum thin films and the application in CIGS solar cell. *Appl. Surf. Sci.* **2016**, *362*, 202–209. [CrossRef]
7. Yoo, H.S.; Kim, J.H. Comparative study of Cu_2ZnSnS_4 film growth. *Sol. Energy Mater. Sol. Cells* **2011**, *95*, 239–244. [CrossRef]
8. Jiang, F.; Shen, H.L. Fabrication and photovoltaic properties of Cu_2ZnSnS_4/i-a-Si/n-a-Si thin film solar cells. *Appl. Surf. Sci.* **2013**, *280*, 138–143. [CrossRef]
9. Peng, C.Y.; Dhakal, T.P.; Garner, S.; Cimo, P.; Lu, S.; Westgate, C.R. Fabrication of Cu_2ZnSnS_4 solar cell on a flexible glass substrate. *Thin Solid Films* **2014**, *562*, 574–577. [CrossRef]
10. Katagiri, H.; Jimbo, K.; Maw, W.S.; Oishi, K.; Yamazaki, M.; Araki, H.; Takeuchi, A. Development of CZTS-based thin film solar cells. *Thin Solid Films* **2009**, *517*, 2455–2460. [CrossRef]
11. Wang, K.; Gunawan, O.; Todorov, T.; Shin, B.; Chey, S.J.; Bojarczuk, N.A.; Mitzi, D.; Guha, S. Thermally evaporated Cu_2ZnSnS_4 solar cells. *Appl. Phys. Lett.* **2010**. [CrossRef]
12. Pawar, S.M.; Inamdar, A.I.; Pawar, B.S.; Gurav, K.V.; Shin, S.W.; Xiao, Y.J.; Kolekar, S.S.; Lee, J.H.; Kim, J.H.; Im, H.S. Synthesis of Cu_2ZnSnS_4 (CZTS) absorber by rapid thermal processing (RTP) sulfurization of stacked metallic precursor films for solar cell applications. *Mater. Lett.* **2014**, *118*, 76–79. [CrossRef]
13. Vanalakar, S.A.; Agawane, G.L.; Shin, S.W.; Suryawanshi, M.P.; Gurav, K.V.; Jeon, K.S.; Patil, P.S.; Jeong, C.W.; Kim, J.Y.; Kim, J.H. A review on pulsed laser deposited CZTS thin films for solar cell applications. *J. Alloys Compd.* **2015**, *619*, 109–121. [CrossRef]
14. Lee, S.G.; Kim, J.M.; Woo, H.S.; Jo, Y.C.; Inamdar, A.I.; Pawar, S.M.; Kim, H.S.; Jung, W.; Im, H.S. Structural, morphological, compositional, and optical properties of single step electrodeposited Cu_2ZnSnS_4 (CZTS) thin films for solar cell application. *Cur. Appl. Phys.* **2014**, *14*, 254–258. [CrossRef]
15. Bhosale, S.M.; Suryawanshi, M.P.; Gaikwad, M.A.; Bhosale, P.N.; Kim, J.H. Influence of growth temperatures on the properties of photoactive CZTS thin films using a spray pyrolysis technique. *Mater. Lett.* **2014**, *129*, 153–155. [CrossRef]
16. Tanaka, K.; Fukui, Y.; Moritake, N.; Uchiki, H. Chemical composition dependence of morphological and optical properties of Cu_2ZnSnS_4 thin films deposited by sol-gel sulfurization and Cu_2ZnSnS_4 thin film solar cell efficiency. *Sol. Energy Mater. Sol. Cells* **2011**, *95*, 838–842. [CrossRef]
17. Swami, S.K.; Kumar, A.; Dutta, V. Deposition of kesterite Cu_2ZnSnS_4 (CZTS) thin films by spin coating technique for solar cell application. *Energy Proc.* **2013**, *33*, 198–202. [CrossRef]
18. Gao, C.; Schnabel, T.; Abzieher, T.; Krammer, C.; Powalla, M.; Kalt, H.; Hetterich, M. $Cu_2ZnSn(S,Se)_4$ solar cells based on chemical bath deposited precursors. *Thin Solid Films* **2014**, *562*, 621–624. [CrossRef]
19. Todorov, T.K.; Tang, J.; Bag, S.; Gunawan, O.; Gokmen, T.; Zhu, Y.; Mitzi, D.B. Beyond 11% efficiency: Characteristics of state-of-the-art $Cu_2ZnSn(S,Se)_4$ solar cells. *Adv. Mater.* **2013**, *3*, 34–38. [CrossRef]
20. Chen, S.Y.; Wang, L.W.; Walsh, A.; Gong, X.G.; Wei, S.H. Abundance of Cu_{Zn} + Sn_{Zn} and $2Cu_{Zn}$ + Sn_{Zn} defect clusters in kesterite solar cell. *Appl. Phys. Lett.* **2012**. [CrossRef]
21. Malerba, C.; Biccary, F.; Ricardo, C.L.A.; Valentini, M.; Chierchia, R.; Muller, M.; Santoni, A.; Esposito, E.; Mangiapane, P.; Scardi, P.; et al. CZTS stoichiometry effects on the band gap energy. *J. Alloys Compd.* **2014**, *582*, 528–534. [CrossRef]
22. Ruan, C.H.; Huang, C.C.; Lin, Y.J.; He, G.R.; Chang, H.C.; Chen, Y.H. Electrical properties of $CuxZnySnS_4$ films with different Cu/Zn ratios. *Thin Solid Films* **2014**, *550*, 525–529. [CrossRef]

23. Kosyak, V.; Karmarkar, M.A.; Scarpulla, M.A. Temperature dependent conductivity of polycrystalline Cu_2ZnSnS_4 thin films. *Appl. Phys. Lett.* **2012**. [CrossRef]
24. Shin, S.W.; Pawar, S.M.; Park, C.Y.; Yun, J.H.; Moon, J.H.; Kim, J.H.; Lee, J.Y. Studies on Cu_2ZnSnS_4 (CZTS) absorber layer using different stacking orders in precursor thin films. *Sol. Energy Mater. Sol. Cells* **2011**, *95*, 3202–3206. [CrossRef]
25. Fairbrother, A.; Fontane, X.; Roca, V.I.; Rodriguez, M.E.; Marino, S.L.; Placidi, M.; Barrio, L.C.; Rodriguez, A.P.; Saucedo, E. On the formation mechanisms of Zn-rich Cu_2ZnSnS_4 films prepared by sulfurization of metallic stacks. *Sol. Energy Mater. Sol. Cells* **2013**, *112*, 97–105. [CrossRef]
26. Birkholz, M. *Thin Film Analysis by X-ray Scattering*; Addison-Wesley: New York, NY, USA, 2006; p. 110.
27. Bhosale, S.M.; Suryawanshi, M.P.; Kim, J.H.; Moholkar, A.V. Influence of copper concentration on sprayed CZTS thin films deposited at high temperature. *Cream. Int.* **2015**, *41*, 8299–8304. [CrossRef]
28. Shinde, N.M.; Deokate, R.J.; Lokhande, C.D. Properties of spray deposited Cu_2ZnSnS_4 (CZTS) thin films. *J. Anal. Appl. Pyrol.* **2013**, *100*, 12–16. [CrossRef]
29. Todorov, T.; Kita, M.; Garda, J.; Escribano, P. Cu_2ZnSnS_4 films deposited by a soft-chemistry method. *Thin Solid Films* **2009**, *517*, 2541–2544. [CrossRef]
30. Inamdar, A.I.; Lee, S.G.; Jeon, K.Y.; Lee, C.H.; Pawar, S.M.; Kalubarme, R.S.; Park, C.J.; Im, H.S.; Jung, W.; Kim, H.S. Optimized fabrication of sputter deposited Cu_2ZnSnS_4 (CZTS) thin films. *Sol. Energy* **2013**, *91*, 196–203. [CrossRef]
31. Kosyok, V.; Mortazavi Amiri, N.B.; Postnikov, A.V.; Scarpulla, M.A. Model of native point defect equilibrium in Cu_2ZnSnS_4 application to one-zone annealing. *J. Appl. Phys.* **2013**. [CrossRef]
32. Long, B.; Cheng, S.Y.; Zheng, Q.; Yu, J.L.; Jai, H.J. Effects of sulfurization time and H_2S concentration on electrical properties of Cu_2ZnSnS_4 films prepared by sol-gel method. *Mater. Res. Bull.* **2016**, *73*, 140–144. [CrossRef]